ORAI1 mutations with distinct channel gating defects in tubular aggregate myopathy

Johann Böhm[1,2,3,4,5]*, Monica Bulla[6]*, Jill E. Urquhart[7,8], Edoardo Malfatti[9,10], Simon G. Williams[7], James O'Sullivan[7,8], Anastazja Szlauer[6], Catherine Koch[1,2,3,4,5], Giovanni Baranello[11], Marina Mora[12], Michela Ripolone[13], Raffaella Violano[13], Maurizio Moggio[13], Helen Kingston[7], Timothy Dawson[14], Christian G. DeGoede[15], John Nixon[16], Anne Boland[17], Jean-François Deleuze[17], Norma Romero[9,10], William G. Newman[7,8], Nicolas Demaurex[6], Jocelyn Laporte[1,2,3,4,5]

[1]Departement of Translational Medicine and Neurogenetics, IGBMC (Institut de Génétique et de Biologie Moléculaire et Cellulaire), 67404 Illkirch, France

[2]Inserm, U964, 67404 Illkirch, France

[3]CNRS, UMR7104, 67404 Illkirch, France

[4]Fédération de Médecine Translationnelle, University of Strasbourg, 67404 Illkirch, France

[5]Collège de France, Chaire de Génétique Humaine, 67404 Illkirch, France

[6]Department of Cell Physiology and Metabolism, University of Geneva, 1211 Geneva, Switzerland

[7]Manchester Centre for Genomic Medicine, St. Mary's Hospital, Manchester M13 9WL, UK

[8]Manchester Centre for Genomic Medicine, University of Manchester, Manchester M13 9WL, UK

[9]Centre de Référence de Pathologie Neuromusculaire Paris-Est, Groupe Hospitalier Pitié-Salpêtrière, 75013 Paris, France

[10]Institut de Myologie, GHU La Pitie-Salpetriere, 75013 Paris, France

[11]Developmental Neurology Unit, Fondazione IRCCS Istituto Neurologico C. Besta, 20133 Milano, Italy

[12]Neuromuscular Diseases and Neuroimmunology Unit, Fondazione IRCCS Istituto Neurologico C. Besta, 20133 Milano, Italy

[13]Neuromuscular and Rare Diseases Unit, Department of Neuroscience, Fondazione IRCCS Ca' Granda, Ospedale Maggiore Policlinico, 20122 Milan, Italy

[14]Department of Pathology, Royal Preston Hospital, Preston PR2 9H7, UK

[15]Department of Paediatric Neurology, Royal Preston Hospital, Preston PR2 9HT, UK

[16]Department of Neurology, Royal Preston Hospital, Preston PR2 9H7, UK

[17]Centre National de Génotypage, Institut de Génomique, CEA, 91057 Evry, France

*These authors contributed equally

Correspondence: Jocelyn Laporte (jocelyn@igbmc.fr)

                    Johann Böhm (johann@igbmc.fr)

                    Tel.: +33 (0)3 88 65 34 12, Fax: +33 (0)3 88 65 32 01

ABSTRACT

Calcium (Ca^{2+}) is a physiological key factor, and the precise modulation of free cytosolic Ca^{2+} levels regulates multiple cellular functions. Store-operated Ca^{2+} entry (SOCE) is a major mechanism controlling Ca^{2+} homeostasis, and is mediated by the concerted activity of the Ca^{2+} sensor STIM1 and the Ca^{2+} channel ORAI1. Dominant gain-of-function mutations in *STIM1* or *ORAI1* cause tubular aggregate myopathy (TAM) or Stormorken syndrome, while recessive loss-of-function mutations are associated with immunodeficiency. Here we report the identification and functional characterization of novel *ORAI1* mutations in TAM patients. We assess basal activity and SOCE of the mutant ORAI1 channels, and we demonstrate that the G98S and V107M mutations generate constitutively permeable ORAI channels, while T184M alters the channel permeability only in the presence of STIM1. These data indicate a mutation-dependent pathomechanism and a genotype/phenotype correlation, as the *ORAI1* mutations associated with the most severe symptoms induce the strongest functional cellular effect. Examination of the non-muscle features of our patients strongly suggest that TAM and Stormorken syndrome are spectra of the same disease. Overall, our results emphasize the importance of SOCE in skeletal muscle physiology, and provide new insights in the pathomechanisms involving aberrant Ca^{2+} homeostasis and leading to muscle dysfunction.

KEYWORDS

Tubular aggregate myopathy, Stormorken syndrome, ORAI1, calcium, SOCE, STIM1

INTRODUCTION

Skeletal muscle physiology directly depends on changes in free cytosolic calcium (Ca^{2+}) levels, and small disturbances in Ca^{2+} homeostasis can severely impact on muscle contraction, differentiation, or gene transcription. A major mechanism controlling Ca^{2+} homeostasis is store-operated Ca^{2+} entry (SOCE), which is triggered by Ca^{2+} store depletion of the endoplasmic/sarcoplasmic reticulum (ER/SR), and results in extracellular Ca^{2+} influx through Ca^{2+} release-activated Ca^{2+} (CRAC) channels as ORAI1 (MIM# 610277). This highly Ca^{2+}-selective plasma membrane channel is composed of tetramers or hexamers forming three concentric rings around the central pore (Hou, et al. 2012; Thompson and Shuttleworth 2013; Cai, et al. 2016). Each ORAI1 subunit is composed of 4 alpha-helical transmembrane domains (M1 to M4) linked by two external (I and III) and one internal (II) loop, with the N- and C-termini facing the cytosol. The M1 transmembrane domain constitutes the ~55 Å long channel pore with an acidic glutamate ring at position E106 forming the selectivity filter and, together with negative residues in the first external loop, conferring high selectivity for Ca^{2+} ions (Vig, et al. 2006; Zhou, et al. 2010; McNally, et al. 2012; Frischauf, et al. 2015). The central segment of the pore contains a rigid hydrophobic

section responsible for the low channel conductance, a gating hinge controlling pore opening, and a basal component potentially avoiding backward Ca^{2+} efflux from the cytoplasm (Zhang, et al. 2011).

Channel opening is mediated through the interaction of the cytoplasmic N- and C-termini of the ORAI1 subunits with STIM1 (MIM# 605921), a transmembrane protein in the ER/SR able to sense luminal Ca^{2+} (Muik, et al. 2008; Navarro-Borelly, et al. 2008; Zheng, et al. 2013). Ca^{2+} store depletion induces a conformational change resulting in oligomerization and cytosolic extension of the STIM1 molecules. The exposure of lipid-binding and channel activating domains (CAD) promotes the accumulation of the STIM1 oligomers at junctional ER/SR structures near the plasma membrane, where they trap and gate the ORAI channels (Luik, et al. 2006; Stathopulos, et al. 2006; Park, et al. 2009).

We previously identified *STIM1* gain-of-function mutations as genetic cause of autosomal dominant tubular aggregate myopathy (TAM, MIM# 160565) (Bohm, et al. 2013). TAM mostly involves elevated creatine kinase (CK) levels and slowly progressive muscle weakness predominantly affecting the proximal muscles of the lower limbs, but also myalgia, cramps, and asymptomatic CK elevation have been described (Bohm, et al. 2013; Bohm, et al. 2014; Hedberg, et al. 2014; Walter, et al. 2015). Muscle biopsies from patients with TAM typically show regular arrays of 70-200 nm long membrane tubules as the main histopathological hallmark (Chevessier, et al. 2005). Tubular aggregates can also arise as secondary features in various inherited and acquired muscle disorders, and accumulate in normal muscle with age (Boncompagni, et al. 2012). All TAM mutations affect highly conserved amino acids in the Ca^{2+}-sensing EF hand domains of STIM1. The only cytosolic STIM1 mutation R304W has been associated with Stormorken syndrome (MIM# 185070), a multisystemic disorder involving tubular aggregate, elevated CK levels, miosis,

thrombocytopenia, ichthyosis, asplenia, dyslexia, and short stature (Misceo, et al. 2014; Morin, et al. 2014; Nesin, et al. 2014). Mutations in *STIM1* causing either TAM or Stormorken syndrome were both shown to induce constitutive STIM1 oligomerization, CRAC channel activation and Ca^{2+} influx in the absence of store depletion (Bohm, et al. 2013; Bohm, et al. 2014; Misceo, et al. 2014; Nesin, et al. 2014). Recently, three gain-of-function mutations causing TAM or a Stormorken-like syndrome were also described in ORAI1 (Nesin, et al. 2014; Endo, et al. 2015). These mutations did not alter ORAI1 localization at the plasma membrane, but resulted in increased SOCE and diminished Ca^{2+}-dependent channel inactivation (CDI).

This study reports the identification of three *ORAI1* gain-of-function mutations (two in the channel pore and one in M3) in patients with TAM with or without isolated characteristics of Stormorken syndrome. Based on clinical, histological, genetic, and functional data, we establish a genotype/phenotype correlation and conclude that TAM and Stormorken syndrome clinically overlap, and have to be considered as spectra of the same disease. We provide the functional evidence that mutations in the first transmembrane domain induce a STIM1-independent permeable Ca^{2+} channel resulting in a more severe phenotype, while the mutation in the third transmembrane domain requires activation through STIM1 to generate an excessive Ca^{2+} influx and causes a milder phenotype, suggesting that the *ORAI1* mutations involve different pathological mechanisms.

MATERIALS AND METHODS

Patients

Sample collection was performed with informed consent from the patients according to the declaration of Helsinki and experimentation was performed following institutional IRB-accepted protocols and the Comité de Protection des Personnes Est IV (DC-2012-1693). Patients were from Honduras (Family 1), the United Kingdom (Family 2), and Italy (Family 3).

Sequencing and segregation analysis

Genomic DNA was prepared from peripheral blood by routine procedures and *STIM1* mutations were excluded by Sanger sequencing. Whole exome sequencing was carried out for patient 11200 from Family 1, and for patients II.1, II.3, and IV.1 from Family 2 using the SureSelect Human All Exon Kit v4 (Agilent, Santa Clara, USA) and the Illumina HiSeq 2000 or 2500 systems (San Diego, USA). Sequence data were aligned to the GRCh37/hg19 reference genome using the Burrows-Wheeler aligner software (http://bio-bwa.sourceforge.net), and variant calling was performed with SAMtools (Li, et al. 2009) or the UnifiedGenotyper (https://www.broadinstitute.org/gatk). Following databases were used for SNP annotation and filtering: Exome Variant Server (http://evs.gs.washington.edu/EVS/), ExAC Browser (http://exac.broadinstitute.org/), dbSNP (http://www.ncbi.nlm.nih.gov/projects/SNP/), 1000 genomes (http://www.1000genomes.org/), as well as the in-house exome databases in Illkirch and Manchester. Impacts of variations were predicted using Alamut v.2.5 (http://www.interactive-biosoftware.com).

For patient 5510 from Family 3, direct Sanger-sequenced for both coding exons of *ORAI1* and the adjacent splice-relevant regions was performed. Segregation analyses for Families 1 and 2 were also performed by Sanger sequencing. The *ORAI1* mutations were numbered according to GenBank NM_032790.3 and NP_116179.2. Nucleotide position reflects cDNA

numbering with +1 corresponding to the A of the ATG translation initiation codon. All identified mutations have been submitted to the LOVD database (http://www.lovd.nl/ORAI1).

Histology and electron microscopy

For histology, transverse sections (10 µm) of the muscle biopsies were stained with modified Gomori Trichrome, NADH tetrazolium reductase (NADH-TR) and Succinic dehydrogenase (SDH) and assessed for fiber morphology, fiber type distribution, and accumulations/infiltrations.

For electron microscopy, muscle sections were fixed in 2.5% paraformaldehyde, 2.5% glutaraldehyde, and 50 mM $CaCl_2$ in 0.1 M cacodylate buffer (pH 7.4). Samples were postfixed with 2% OsO_4, 0.8% $K_3Fe(CN)_6$ in 0.1 M cacodylate buffer (pH 7.4) for 2 h at 4 °C and incubated with 5% uranyl acetate for 2 h at 4 °C. Muscles were dehydrated in a graded series of ethanol and embedded in epon resin. Thin sections were examined with an electron microscope (Philips CM120, FEI Company, Hillsboro, USA).

Protein studies

Immunofluorescence was performed with routine protocols using following antibodies: rabbit anti-Orai1 (Abcam, Paris, France), mouse anti-GOK/Stim1 (BD Biosciences, Franklin Lakes, USA), mouse Anti-Ryanodine receptor Clone 34C Product R-12 (Sigma-Aldrich, Saint Louis, USA), NCL-SERCA2 mouse monoclonal antibody, clone IID8 (Novocastra, Newcastle, UK). Sections were mounted with antifade reagent (Invitrogen, Carlsbad, USA) and viewed using a laser scanning confocal microscope (TCS SP2; Leica Microsystems, Wetzlar, Germany).

Constructs

The human ORAI-eGPF and mCherry-STIM1 constructs were kind gifts from Liangyi Chen (Beijing University, China) and Richard S. Lewis (Stanford University, USA). The *ORAI1* point mutations (c.292G>A, c.319G>A, c.551C>T) were introduced by site-directed mutagenesis using the *Pfu* DNA polymerase (Stratagene, La Jolla, USA). The plasmid carrying an untagged STIM1 was purchased from OriGene (NM_003156; OriGene Technologies, Rockville, USA), and the control vector pEGFP-C1 from Clontech (Palo Alto, CA).

Cells and transfections

Stim1$^{-/-}$/Stim2$^{-/-}$ mouse embryonic fibroblasts (MEF-DKO), generated by targeted gene disruption, were a kind gift from Masatsugu Oh-Hora (Tokyo Medical and Dental University, Japan), and HEK-293T cells were purchased from ATCC (CRL-11268; Manassas, USA). MEF-DKO and HEK-293T cells were respectively cultured in DMEM 15140-122 and 31966-021 (Gibco Life Technologies, Carlsbad, USA) supplemented with 10% fetal bovine serum (10270-106, Gibco Life Technologies), 5 μg/ml streptomycin and 5 units/ml penicillin (15140-122, Gibco Life Technologies), and were maintained at 37 °C in 5 % CO_2. Cells were seeded on poly-L-lysine (P4832; Sigma-Aldrich) coated glass coverslips, and transfected at 50% confluency with Lipofectamine® 2000 (11668-019; Invitrogen). For co-expression experiments, mCherry-STIM1 and ORAI1-eGFP constructs were transfected in a 3:1 ratio by mass. For cells transfected with the ORAI1-eGFP G98S mutant and the respective controls, low Ca^{2+} containing medium (0.2 mM $CaCl_2$) was used to prevent Ca^{2+} toxicity. All subsequent experiments were performed within 24h post transfection.

TIRF microscopy

To assess the impact of the *ORAI1* mutations on the channel distribution at the plasma membrane (PM), HEK-293T cells were co-transfected with wild type (WT) or mutated ORAI1-eGFP and an untagged STIM1 construct, and cultured overnight in low Ca^{2+} containing medium complemented with 5 µM lanthanum. The TIRF plane was determined according to the PM GFP fluorescence at resting state, and images were collected by a Nikon Eclipse Ti microscope (Tokyo, Japan) equipped with a Perfect Focus System, a 100x 1.49 Oil CFI Apochromat TIRF objective and a cooling EMCCD iXon camera (DU-897E-CS0-#BV-500; Andor Technology Ltd, Belfast, Northern Ireland). Cells were excited with a 488 nm 50 mW laser and light was collected through the TIRF Quad dichroic beamsplitter 405/488/561/640 and the emission filter FITC 525/50 from Nikon. The experiment was performed at room temperature. Cells were treated with 1 µM Thapsigargin (Sigma-Aldrich) to follow the kinetics of ORAI1 clustering at the PM. Live images were acquired with the NIS-Elements AR software V4.30.02 (Nikon), and ORAI1 clusters were quantified and characterized with a granularity detection journal on Metamorph software 7.8.12.0 (Molecular Devices, Sunnyvale, USA) after background subtraction. Regions containing clusters were identified at the end of each experiment and their increasing intensities were plotted over time. The results were normalized as follows: $Fc_{(t=n)} = (Fcr_{(t=n)} - Frr_{(t=n)})$; $F/F0_{(t=n)} = (\Sigma\ Fc_{(t=n)}/nb.\ clusters + Frr_{(t=0)})/\ Frr_{(t=0)}$, where $Fc_{(t=n)}$ is the fluorescence intensity of a cluster at a given time, $Fcr_{(t=n)}$ the intensity measured in a region that will contain a cluster following store depletion, and $Frr_{(t=n)}$ the intensity of a reference region devoid of clusters throughout the experiment. The average fluorescence intensity of cumulated clusters at the cellular level ($F_{(t=n)}$) was normalized to the fluorescence of the empty region at the beginning of the experiment ($F0=Frr_{(t=0)}$). The percentage of the PM covered by clusters (density) was determined as the summed area of clusters divided by the total surface of the PM visible in the TIRF plane.

Ca^{2+} measurements

To assess cytosolic Ca^{2+} levels, cells were loaded at room temperature with 4 µM of the Ca^{2+} sensor Fura-2 AM and 1 µM Pluronic acid F-127 (F-1201 and P-3000MP; Invitrogen) in 2 or 0.2 mM CaCl$_2$ recording solution. After 30 minutes in the dark, cells were washed and allowed for de-esterification for at least 15 min. Fura-2 ratiometric fluorescence emission was recorded with an Axio Observer microscope (Zeiss, Jena, Germany) equipped with a Lambda DG4 175 watts xenon arc lamp (Sutter Instrument Company, Novato, USA) and a rapidly changing filter wheel (Ludl Electronic Products, München, Germany). Excitation filters 340AF15 and 380AF15 were purchased from Omega Optical (Brattleboro, USA). Exposure time was 500 ms every 3 seconds for each wavelength. Emission was collected through the dichroic/filter couple 415DCLP/510WB40 (Omega Optical), by a 12-bit CCD cooling camera (CoolSnap HQ, Ropper Scientific, Trenton, USA) with a 2x gain and a binning of 4. To measure store-operated Ca^{2+} entry, 1 µM Thapsigargin was used to passively deplete the Ca^{2+} stores. For Mn^{2+} quenching experiments, 500 µM Mn^{2+} were added while cells were excited at 360 nm (360BP10, Omega Optical). Recording solutions contained 140 mM NaCl, 5 mM KCl, 1 mM MgCl$_2$, 10 mM Hepes, 10 mM D-(+)-glucose and the indicated amounts of CaCl$_2$. The Ca^{2+}-free solution contained 1 mM EGTA instead of CaCl$_2$. The pH was adjusted to 7.4 at 37 °C with NaOH. All experiments were achieved at 37 °C with pre-heated solutions. Ca^{2+} recordings were acquired and analyzed with the Metafluor 6.3 software (Universal Imaging, West Chester, USA) after background subtraction. For cells co-expressing mCherry-STIM1 and ORAI1-eGFP constructs, only cells with a mCherry/eGFP fluorescence ratio above 1 were analyzed.

Statistics

GraphPad Prism 6.05 was used for statistical evaluation of the data. Statistical significance was determined by the two-tailed unpaired Student's test with systematic Welch correction for variance.

RESULTS

Clinical reports

The patients characterized in this study belong to three unrelated families with a broad range of symptoms and signs with different ages of onset and disease severity, but sharing prominent tubular aggregates on muscle biopsies as the main histopathological hallmark. Patient 11200 (Family 1) is a singleton, Family 2 has an ancestral history of a muscle phenotype segregating as a dominant disease over at least four generations, and Family 3 displays a mother to son disease inheritance (clinical features summarized in Table 1).

Patient 11200 from Family 1 is now 12 years old. Pregnancy, birth and neonatal history were uneventful, although motor milestones were slightly delayed. The patient achieved sitting at the age of 8 months, and independent walking at 24 months. Tip-toe-walking and frequent falls were noticed since age 2, and contractures of elbows and Achilles tendons were diagnosed in the following years. Clinical examination at the age of 10 revealed ichthyosis, stiffness, proximal muscle weakness and reduced tendon reflexes of the lower limbs. The patient was unable to jump, and had a waddling gait. He reported cramps and myalgia, both at rest and after exercise, headaches, and frequent episodes of bleeding from mouth, nose, and bowel. He had anemia but not thrombocytopenia, and blood calcium levels were repeatedly normal or only mildly reduced. Eye examination showed miosis, heart and lung functions were normal, and cognitive assessment showed results within the normal range. CK levels

were repeatedly elevated, with values up to 2052 U/l. Motor nerve conduction velocities were normal and EMG showed chronic neurogenic abnormalities and mild myopathic changes in the proximal lower limbs. Muscle MRI revealed fibro-fatty replacements in the posterior and medial compartments of the thigh and of the posterior compartment of the calf (Supp. Figure S1). Abdominal ultrasound excluded asplenia/hyposplenia. The parents and the younger sister are healthy.

For Family 2, five affected members underwent regular clinical examinations. They are now between 6 and 47 years old, and pregnancy, birth, and early childhood was normal for all. Slightly delayed motor milestones as well as slight dyslexia were reported for patients IV.1, and IV.2, and might have been overlooked for the older generations. All showed tip-toe walking associated to Achilles tendon contractures by the age of 8 years. Only the youngest patient, now 6 years old, does not show tip-toe walking. The proximal muscle of the lower limbs were predominantly affected, and involved weakness (II.1, III.1, III.2), stiffness (II.1, III.2), cramps (II.1, III.2), and myalgia (II.1, III.1, IV.1, IV.2). All had difficulties running and climbing stairs. Calf hypertrophy was noted for patients III.1 and IV.1. CK levels were elevated for all and ranged between 484 and 1538 U/I. Motor nerve conduction velocity, assessed for patient III.1 was normal, and EMG showed myopathic changes.

Patient 5510 from Family 3 was diagnosed with asymptomatic hyperCKemia through routine blood tests at the age of 56. Medical examination at age 60 revealed mild general muscle weakness, and the patient reported myalgia of the lower limbs and cramps, but motor nerve conduction velocity and EMG did not reveal any abnormalities. The patient also presented with hypereosinophilia resulting from allergic diathesis, pectus excavatum, and arched palate. CK levels were repeatedly elevated and ranged between 400 and 600 U/I, and his mother was also reported to have asymptomatic hyperCKemia.

13

Histology and ultrastructural analyses reveal tubular aggregates

Muscle biopsies from all patients described in this study displayed tubular aggregates appearing on Gomori trichrome and on NADH-TR staining (Figure 1). In agreement with previously described TAM cases, the aggregates are less detectable with SDH, suggesting a reticulum and not a mitochondrial origin (Chevessier, et al. 2005; Bohm, et al. 2013). Aggregates were observed in both fiber types in all analyzed biopsies. Additional observations comprise fiber size variability and internalized nuclei.

Ultrastructural analyses demonstrated that the tubular aggregates are of variable size and consist of single or double-walled membranes of different diameter (Figure 1). Overall, the histological and ultrastructural features of the biopsies were strikingly similar and strongly suggestive of tubular aggregate myopathy.

Exome sequencing identifies mutations in *ORAI1*

Sanger sequencing of the known TAM gene *STIM1* did not reveal any putative pathogenic variant in the families described here. We performed exome sequencing for Families 1 and 2, and identified heterozygous missense mutations in *ORAI1*. Patient 11200 from Family 1 carries the *ORAI1* c.292G>A (p.Gly98Ser) *de novo* mutation in exon 1, and the affected members of Family 2 harbor the *ORAI1* c.319G>A (p.Val107Met) mutation in exon 2 (Figure 2A). Another missense mutation (c.551C>T; p.Thr184Met) in exon 2 was found by direct *ORAI1* Sanger sequencing of patient 5510 from Family 3. None of the three mutations was found in the available healthy family members and none was listed in the public or internal SNP databases. However, the p.Gly98Ser mutation was previously described in an unrelated Japanese family with TAM involving diffuse muscle weakness, joint contractures, a rigid spine and hypocalcaemia (Endo, et al. 2015).

14

All three missense mutations affect highly conserved amino acids in ORAI1 (Figure 2B) The mutations p.Gly98Ser and p.Val107Met affect amino acids in M1, and p.Thr184Met affects an amino acid in M3 (Figure 2C). M1 forms the ion conduction pathway, while M2 and M3 encircle the pore and are surrounded by the M4 outer ring (Hou, et al. 2012; Frischauf, et al. 2015). The residue G98 is located in the rigid section of the channel responsible for ion conduction, and the residue V107 neighbors E106, involved in Ca^{2+} selectivity.

Tubular aggregates contain STIM1

To characterize the structure and composition of the tubular aggregates associated with *ORAI1* mutations, we performed immunolocalization experiments on muscle biopsies from patient 11200 (Family 1) and II.1 (Family 2) (Figure 1). We previously showed that tubular aggregates in TAM patients with *STIM1* mutations contain various SR proteins as STIM1, the Ca^{2+} channel RYR1 (MIM# 180901), the RYR1-effector triadin (MIM# 603283), or the Ca^{2+} pump SERCA (MIM# 108730), and that RYR1 and STIM1 are exclusively found in the aggregate periphery (Bohm, et al. 2013). In agreement with our previous observations, the aggregates in the TAM patients with *ORAI1* mutations also contain SERCA, and RYR1 is mainly found in the periphery of the aggregates (Figure 1). The aggregates display strong STIM1 signals, thereby linking *STIM1* and *ORAI1*-related TAM. Of note, STIM1 signals are not restricted to the aggregate periphery; this is in contrast to the immunolocalization experiments in *STIM1* patients, and might reflect different ways of tubular aggregate formation in patients with *STIM1* or *ORAI1* mutation. Aggregated ORAI1 is barely or not detectable on the biopsies of the analyzed patients, supporting the idea that tubular aggregates essentially consist of sarcoplasmic reticulum membrane and proteins.

ORAI1 mutants traffic normally to plasma membrane clusters

In order to assess the impact of the three *ORAI1* mutations on channel localization and trafficking, we generated wild type (WT) and ORAI1-eGFP G98S, V107M, and T184M constructs, exogenously co-expressed them with human STIM1 in HEK-293T cells, and imaged the formation of ORAI1 clusters at the PM by total internal reflection fluorescence (TIRF) microscopy. WT and mutant ORAI1 were homogenously distributed in the TIRF plane in resting cells, and accumulated in clusters following depletion of ER Ca^{2+} stores with the SERCA inhibitor Thapsigargin (Tg) (Figure 3A). The intensity of the clusters and the extent of cell membrane covered by clusters was comparable in cells expressing WT or mutant ORAI1 at resting or activated state (Figure 3B and 3C). We therefore conclude that the mutations do not significantly alter the ORAI1 localization at the plasma membrane, nor its clustering upon SOCE activation.

ORAI1 mutations produce constitutively active channels

To evaluate the impact of the *ORAI1* mutations on the basal channel activity, we measured the cytosolic Ca^{2+} levels ($[Ca^{2+}]_{cyt}$) in HEK-293T cells transfected with the ORAI1-eGFP constructs, and loaded with the ratiometric Ca^{2+} sensor Fura-2, AM. Cells were sequentially exposed to Ca^{2+}-rich and Ca^{2+}-poor media to assess the extent of Ca^{2+} entry across the channel in cells with replete stores (Figures 4A-C). Mean basal Fura-2 ratio values were elevated in cells expressing ORAI1 V107M (0.52, SD $\pm$ 0.14) or T184M (0.48, SD $\pm$ 0.10) compared to cells expressing WT ORAI1 (0.39, SD $\pm$ 0.08), and decreased significantly upon Ca^{2+} removal. HEK-293T cells expressing the ORAI1 G98S construct displayed extremely high $[Ca^{2+}]_{cyt}$ in Ca^{2+}-rich conditions and were cultured in 0.2 mM $CaCl_2$ to minimize cytotoxicity. Under these conditions, mean basal Fura-2 ratio was significantly elevated (0.68, SD $\pm$ 0.19, compared to WT 0.35, SD $\pm$ 0.03), decreased upon Ca^{2+} removal, and markedly increased upon addition of 2 mM Ca^{2+} (1.28, SD $\pm$ 0.20, compared to WT 0.36, SD

$\pm$ 0.04, Figures 4B and 4C). These results suggest that the mutated ORAI1 channels are Ca^{2+} permeable even in the absence of store depletion, with a more pronounced degree of permeability for G98S compared to V107M or T184M ORAI1.

G98S and V107M alter ORAI1 activity independently of STIM1

In order to assess the STIM-dependence of the constitutive activation of mutant ORAI1 channels, we next transfected mouse embryonic fibroblasts bearing a targeted disruption in the *Stim1* and *Stim2* genes (MEF-DKO). Since steady-state $[Ca^{2+}]_{cyt}$ reflects the combined activity of Ca^{2+} pumps, channels and exchangers, we used the Mn^{2+} quench assay (Figures 4D-F). Mn^{2+} permeates through Ca^{2+} channels and quenches the Fura-2 fluorescence, thereby allowing the individual quantification of the influx component. In these experiments, we observed a massive Mn^{2+} influx in MEF-DKO cells expressing ORAI1-eGFP V107M or G98S, while only a small Mn^{2+} influx was detectable in cells expressing ORAI1-eGFP T184M or WT, with no significant difference among these two conditions. Similar results were obtained by measuring the amplitude of the Ca^{2+} elevation evoked by the readmission of 2 mM Ca^{2+} to MEF-DKO cells treated with Tg (Supp. Figure S2), where Fura-2 ratio increase was observed only in cells expressing G98S or V107M ORAI1. In conclusion, G98S and V107, but not T184M ORAI1 channels appear constitutively active in the absence of STIM proteins. Accordingly, Mn^{2+} quench experiments in HEK-293T cells endogenously expressing STIM1 and STIM2 demonstrated that cells transfected with any of the mutant channels including ORAI1-T184M displayed significant cation entry (Supp. Figure S3).

The ORAI1 mutants mediate excessive Ca^{2+} entry when gated by STIM1

To test whether the *ORAI1* mutations also impact on the STIM1-gated maximal channel activity, we co-transfected HEK-293T cells with mCherry-STIM1 and WT or mutated

ORAI1-eGFP constructs. We induced passive reticular Ca^{2+} depletion through Tg treatment in Ca^{2+}-free medium, and measured SOCE upon readmission of 0.5 mM Ca^{2+} to the medium. Cells expressing any of the ORAI1 mutants displayed significantly increased SOCE with 2-3 fold steeper slope of Fura-2 ratio increase compared to cells expressing WT ORAI1 (Figures 5A and 5B). Analysis of the response kinetics 60 s after Ca^{2+} admission demonstrated a 30 % Fura-2 ratio decrease for cells transfected with WT or T184M ORAI1, while the ratio remained at near maximal levels in cells expressing G98S or V107M ORAI1 (Figure 5C).

To specifically assign ORAI1 channel activation to STIM1, we repeated the co-expression experiments in MEF-DKO cells (Figures 5D-F). Following Tg treatment and readmission of Ca^{2+}, cells co-expressing STIM1 and V107M or T184M ORAI1 mutants displayed a strongly increased SOCE slope compared to cells co-expressing STIM1 and WT ORAI1. Expression of a control vector did not affect the Ca^{2+} response of the recipient cells, and expression of STIM1 alone fully restored SOCE in the MEF-DKO cells (Supp. Figure S2). Unexpectedly, MEF-DKO expressing STIM1 and WT or G98S ORAI1 and cultured in low Ca^{2+} exhibited a high SOCE slope (Figures 5D-E), potentially reflecting a specific adaptation of these cells to Ca^{2+} deprivation, and resulting in a more efficient activation of the SOCE pathway. However, and in agreement with the results obtained in transfected HEK-293T cells, the Fura-2 ratio remained elevated 60 s post Ca^{2+} readmission in cells expressing the G98S and V107M mutants while the ratio decreased in cells expressing T184M ORAI1 (Figure 5F).

Overall and in accordance with the Mn^{2+} quenching data, these results strongly indicate a mutation-dependent pathomechanism. All three ORAI1 mutations G98S, V107M, and T184M involve maximal SOCE in presence of active STIM1, but only G98S and V107M generate a constant Ca^{2+} influx independently of STIM1 activation.

DISCUSSION

Here we report three *ORAI1* mutations causing tubular aggregate myopathy, and we support our findings by clinical, histological, genetic and functional data. Our patients presented with different age of onset, disease severity, and additional non-muscular features, suggesting that TAM and Stormorken syndrome are spectra of the same disease. We functionally demonstrate for the first time that the mutations in different ORAI1 transmembrane domains appear to involve different pathomechanisms, and thereby uncover a genotype-phenotype correlation.

Tubular aggregates in *ORAI1* patients contain STIM1

As both *STIM1* and *ORAI1* mutations lead to TAM, we compared the structure and composition of the tubular aggregates in our *ORAI1* patients with the published *STIM1* patients (Bohm, et al. 2013). The tubular aggregates in *STIM1* patients were shown to contain diverse sarcoplasmic reticulum proteins as RYR1, triadin, SERCA, and STIM1, and STIM1 was mainly found in the periphery of the aggregates (Bohm, et al. 2013). Immunohistofluorescence on muscle sections from *ORAI1* patients also demonstrated the presence of STIM1 and other sarcoplasmic reticulum proteins in the aggregates. This observation provides a link between *STIM1* and *ORAI1*-related TAM at the histopathological level, and suggests that secondary STIM1 aggregation plays a role in the pathogenesis of *ORAI1* mutations. Of note, the STIM1 signals were detectable in the periphery as well as in the center of the aggregates, potentially reflecting a difference in tubular aggregate formation in patients with *STIM1* and *ORAI1* mutation. Even if mutated, the plasma membrane Ca^{2+} channel ORAI1 is barely or not detectable in the aggregates, confirming that the tubular aggregates are primarily of sarcoplasmic reticulum origin. Considering the increased Ca^{2+} entry resulting from *STIM1* or *ORAI1* mutations, we might speculate that the excessive

cellular Ca^{2+} is in large parts stored in the reticulum, provoking reticular overload and dilatation, and resulting in cisternal pinching off to form the primary stage of the tubular aggregates. This is line with the observation that tubular aggregates contain large amounts of Ca^{2+} (Salviati, et al. 1985; Chevessier, et al. 2005).

ORAI1 mutations involve different pathomechanisms

To mechanistically investigate the impact of the ORAI1 G98S, V107M, and T184M mutations, we analyzed the channel activity in presence or absence of STIM1. Expression of any of the mutant ORAI1-eGFP constructs in HEK-293T cells resulted in elevated basal Ca^{2+} levels, but in mouse fibroblasts devoid of STIM (*Stim1$^{-/-}$/Stim2$^{-/-}$*), only G98S and V107M induced significant cation influx in the Mn^{2+} quench assay. This demonstrates that both G98S and V107M ORAI1 channels are constantly permeable for Ca^{2+}, while the overactivity of the T184M ORAI1 channel is conditioned by the presence of STIM. Accordingly, and considering that the constant fluctuation of Ca^{2+} levels within cellular compartments results in a varying sub-pool of activated STIM1/STIM2, and that STIM2 with is lower Ca^{2+} affinity and higher lipid-binding avidity has been shown to be pre-recruited to the cortical ER at basal ER Ca^{2+} concentrations (Parvez, et al. 2008), the endogenous STIM proteins in HEK-293T cells might be sufficient to partially activate the T184M ORAI1 channel. It is possible that the T184M mutation increases the binding sensitivity of the channel to STIM1 and STIM2 or to the transient receptor potential canonical (TRPC) channels to form a ternary complex with STIM1 at the plasma membrane (Lu, et al. 2010), which might explain the higher basal Ca^{2+} level in cells expressing the T184M mutant even in the absence of store depletion. The extensive characterization of the T184M mutation might reveal a residue or domain regulating STIM-mediated channel gating. Excessive Ca^{2+} entry was also reported for other

ORAI1 mutations (Nesin, et al. 2014; Endo, et al. 2015), but the STIM-dependence of the channel activation was not investigated in these studies.

Further evidence for a different pathomechanism of the *ORAI1* mutations comes from the co-expression experiments. HEK-293T or MEF-DKO cells co-expressing mCherry-STIM1 and any of the ORAI1-eGFP mutants induced excessive Ca^{2+} influx following SOCE activation, but only G98S and V107M generated a continuous and long lasting Ca^{2+} influx. In contrast, Ca^{2+} influx significantly decreased over time in HEK-293T or MEF-DKO cells co-expressing STIM1 and T184M ORAI1. This discrepancy potentially reflects a difference in Ca^{2+}-dependent inactivation (CDI) of the mutant channels and/or their dissociation kinetics from STIM1. Alternatively, the higher basal Ca^{2+} levels in cells expressing ORAI1 G98S or V107M might increase the threshold triggering CDI or Ca^{2+} extrusion. It is also possible that the G98S and V107M mutations directly or indirectly impact on the Ca^{2+} extrusion systems.

In summary, our results suggest a mutation-specific pathomechanism. G98S and V107M induce constitutive channel opening independently of STIM, while T184M overactivation is conditioned by the presence of STIM. In accordance, the amino acid G98 resides in the hydrophobic gating hinge, and V107 locates near the Ca^{2+} selectivity filter of the M1 transmembrane domain (Zhou, et al. 2010; Hou, et al. 2012). Disturbance of these key functions is expected to impact on ion flow, which is confirmed by our functional data demonstrating constitutive Ca^{2+} permeability independently of STIM. This conclusion is also sustained by similar findings based on the functional characterization of artificial M1 mutations (Zhang, et al. 2011). Conversely, T184 is not located in the channel pore, and the STIM-dependent overactivation of the mutant channel strongly suggests that transmembrane domain M3 is directly or indirectly implicated in STIM-mediated ORAI1 gating.

ORAI1 mutations in M1 induce a more severe phenotype

Considering the clinical presentation of our and all previously published patients with activating *ORAI1* mutations (Nesin, et al. 2014; Endo, et al. 2015), the most severe muscle phenotypes result from mutations in M1, a moderate muscle phenotype from a mutation in M2, and milder muscle phenotypes from mutations in M3 and M4. This correlates well with our functional data, demonstrating a stronger impact of M1 mutations on channel function.

Our patients were diagnosed with tubular aggregate myopathy based on biochemical blood tests and histological findings. All displayed repeatedly elevated serum CK levels in combination with prominent tubular aggregates as the major structural aberration on muscle biopsies. The clinical presentation was however variable, ranging from severe early-onset muscle weakness and contractures (patient 11200 from Family 1) to mild late-onset muscle weakness (patient 5510 from Family 3). A similar interfamilial variability was recently described for other families with *ORAI1* mutations. G98S was described in two Japanese family presenting childhood-onset TAM, joint contractures, hypocalcaemia, rigid spine, and elevated CK levels (Endo, et al. 2015). We identified the same mutation in our unrelated Family 1, and the clinical manifestations were comparable. The same study reported a third Japanese family harboring the *ORAI1* L138F mutation, and presenting with weaker clinical features involving adolescence-onset TAM, minor joint contractures, and slightly elevated CK levels. In addition, a family carrying the ORAI1 P245L mutation was described with late-onset TAM and increased CK levels (Nesin, et al. 2014).

Taking into account the clinical manifestation of all TAM patients with *ORAI1* mutation, our functional data, and the published ORAI1 protein structure, we conclude that mutations affecting the pore lead to constitutive channel permeability, and result in early-onset muscle weakness often associated with contractures. In contrast, mutations affecting the concentric

channel rings involve a STIM-dependent overactivity of ORAI1, and result in less severe symptoms with minor muscle weakness.

ORAI1 patients present discrete signs of Stormorken syndrome

Tubular aggregate myopathy in combination with miosis, thrombocytopenia, asplenia, ichthyosis, dyslexia/intellectual disability, and short stature defines Stormorken syndrome. Both TAM and Stormorken syndrome are caused by gain-of-function mutations in *STIM1* and *ORAI1* (Bohm, et al. 2013; Misceo, et al. 2014; Morin, et al. 2014; Nesin, et al. 2014; Endo, et al. 2015). To explore the possibilities that TAM and Stormorken syndrome are either different nosological entities or spectra of the same disease, we examined our patients for non-muscle phenotypes and reviewed the published *ORAI1* cases. We noticed miosis (patient 11200, Family 1, and (Nesin, et al. 2014)), frequent episodes of bleeding (patient 11200, Family 1), ichthyosis, (patient 11200, Family 1), and dyslexia/intellectual disability (patients IV.1, and IV.2, Family 2, Family A (Endo, et al. 2015)). These data show that signs of Stormorken syndrome are found in many patients with activating *ORAI1* mutations, and we conclude that TAM and Stormorken syndrome are spectra of the same disease. This is of high importance for genetic diagnosis and counseling, as *ORAI1* mutations should be considered in patients with elevated CK levels and prominent tubular aggregates on muscle biopsies, especially if they present signs of Stormorken syndrome.

Overactive SOCE versus underactive SOCE in Mendelian disorders

STIM1 and ORAI1 act within the same SOCE pathway regulating Ca^{2+} homeostasis in various tissues. The identification of gain-of-function mutations in *STIM1* and *ORAI1* represents a strong proof for the implication of aberrant SOCE in the development of

TAM/Stormorken syndrome. This is sustained by our functional and immunolocalization studies demonstrating a pathomechanistic link between both proteins.

While heterozygous gain-of-function mutations in *STIM1* or *ORAI1* generate excessive Ca^{2+} influx and result in the development of TAM/Stormorken syndrome (Bohm, et al. 2013; Bohm, et al. 2014; Hedberg, et al. 2014; Misceo, et al. 2014; Morin, et al. 2014; Nesin, et al. 2014; Endo, et al. 2015; Markello, et al. 2015), homozygous loss-of-function mutations in either of the genes suppress Ca^{2+} influx and are associated with severe immunodeficiency (Feske, et al. 2006; McCarl, et al. 2009; Picard, et al. 2009; Byun, et al. 2010; Fuchs, et al. 2012; Lacruz and Feske 2015) (MIM# 612782, # 612783). We conclude that strict regulation of Ca^{2+} homeostasis ensures normal physiology of muscle, leucocytes, platelets, skin, and other cells and tissues, and that overactive SOCE causes tubular aggregate myopathy/Stormorken syndrome, while underactive SOCE causes immunodeficiency.

Conclusions

Our work indicates for the first time a mutation-specific pathomechanism for *ORAI1* gain-of-function mutations, thereby uncovers a clear genotype-phenotype correlation, and improves the understanding of the pathology of TAM/Stormorken syndrome and store-operated Ca^{2+} entry, altered in rare and common diseases.

CONFLICT OF INTEREST

None of the authors reports conflict of interest.

ACKNOWLEDGEMENTS

AUTHOR CONTRIBUTIONS

JB, WGN, ND, and JL designed and coordinated the study. JB, MB, JU, EM, SGW, JO, AS, CK, and WGN performed the experiments. GB, MM, WGN, MR, RV, MM, HK, TD, CGD, JN, and NBR contributed clinical samples, histological and patient data. JB, MB, ND and JL wrote the manuscript.

REFERENCES

Bohm J, Chevessier F, Koch C, Peche GA, Mora M, Morandi L, Pasanisi B, Moroni I, Tasca G, Fattori F, et al. 2014. Clinical, histological and genetic characterisation of patients with tubular aggregate myopathy caused by mutations in STIM1. J Med Genet 51:824-833.

Bohm J, Chevessier F, Maues De Paula A, Koch C, Attarian S, Feger C, Hantai D, Laforet P, Ghorab K, Vallat JM, et al. 2013. Constitutive activation of the calcium sensor STIM1 causes tubular-aggregate myopathy. Am J Hum Genet 92:271-278.

Boncompagni S, Protasi F, Franzini-Armstrong C. 2012. Sequential stages in the age-dependent gradual formation and accumulation of tubular aggregates in fast twitch muscle fibers: SERCA and calsequestrin involvement. Age (Dordr) 34:27-41.

Byun M, Abhyankar A, Lelarge V, Plancoulaine S, Palanduz A, Telhan L, Boisson B, Picard C, Dewell S, Zhao C, et al. 2010. Whole-exome sequencing-based discovery of STIM1 deficiency in a child with fatal classic Kaposi sarcoma. J Exp Med 207:2307-2312.

Cai X, Zhou Y, Nwokonko RM, Loktionova NA, Wang X, Xin P, Trebak M, Wang Y, Gill DL. 2016. The Orai1 Store-operated Calcium Channel Functions as a Hexamer. J Biol Chem.

Chevessier F, Bauche-Godard S, Leroy JP, Koenig J, Paturneau-Jouas M, Eymard B, Hantai D, Verdiere-Sahuque M. 2005. The origin of tubular aggregates in human myopathies. J Pathol 207:313-323.

Endo Y, Noguchi S, Hara Y, Hayashi YK, Motomura K, Miyatake S, Murakami N, Tanaka S, Yamashita S, Kizu R, et al. 2015. Dominant mutations in ORAI1 cause tubular aggregate myopathy with hypocalcemia via constitutive activation of store-operated Ca(2)(+) channels. Hum Mol Genet 24:637-648.

Feske S, Gwack Y, Prakriya M, Srikanth S, Puppel SH, Tanasa B, Hogan PG, Lewis RS, Daly M, Rao A. 2006. A mutation in Orai1 causes immune deficiency by abrogating CRAC channel function. Nature 441:179-185.

Frischauf I, Zayats V, Deix M, Hochreiter A, Jardin I, Muik M, Lackner B, Svobodova B, Pammer T, Litvinukova M, et al. 2015. A calcium-accumulating region, CAR, in the channel Orai1 enhances Ca(2+) permeation and SOCE-induced gene transcription. Sci Signal 8:ra131.

Fuchs S, Rensing-Ehl A, Speckmann C, Bengsch B, Schmitt-Graeff A, Bondzio I, Maul-Pavicic A, Bass T, Vraetz T, Strahm B, et al. 2012. Antiviral and regulatory T cell immunity in a patient with stromal interaction molecule 1 deficiency. J Immunol 188:1523-1533.

Hedberg C, Niceta M, Fattori F, Lindvall B, Ciolfi A, D'Amico A, Tasca G, Petrini S, Tulinius M, Tartaglia M, et al. 2014. Childhood onset tubular aggregate myopathy associated with de novo STIM1 mutations. J Neurol.

Hou X, Pedi L, Diver MM, Long SB. 2012. Crystal structure of the calcium release-activated calcium channel Orai. Science 338:1308-1313.

Lacruz RS, Feske S. 2015. Diseases caused by mutations in ORAI1 and STIM1. Year in Immunology 1356:45-79.

Li H, Handsaker B, Wysoker A, Fennell T, Ruan J, Homer N, Marth G, Abecasis G, Durbin R. 2009. The Sequence Alignment/Map format and SAMtools. Bioinformatics 25:2078-2079.

Lu M, Branstrom R, Berglund E, Hoog A, Bjorklund P, Westin G, Larsson C, Farnebo LO, Forsberg L. 2010. Expression and association of TRPC subtypes with Orai1 and STIM1 in human parathyroid. J Mol Endocrinol 44:285-294.

Luik RM, Wu MM, Buchanan J, Lewis RS. 2006. The elementary unit of store-operated Ca2+ entry: local activation of CRAC channels by STIM1 at ER-plasma membrane junctions. J Cell Biol 174:815-825.

Markello T, Chen D, Kwan JY, Horkayne-Szakaly I, Morrison A, Simakova O, Maric I, Lozier J, Cullinane AR, Kilo T, et al. 2015. York platelet syndrome is a CRAC channelopathy due to gain-of-function mutations in STIM1. Mol Genet Metab 114:474-482.

McCarl CA, Picard C, Khalil S, Kawasaki T, Rother J, Papolos A, Kutok J, Hivroz C, Ledeist F, Plogmann K, et al. 2009. ORAI1 deficiency and lack of store-operated Ca2+ entry cause immunodeficiency, myopathy, and ectodermal dysplasia. J Allergy Clin Immunol 124:1311-1318 e1317.

McNally BA, Somasundaram A, Yamashita M, Prakriya M. 2012. Gated regulation of CRAC channel ion selectivity by STIM1. Nature 482:241-245.

Misceo D, Holmgren A, Louch WE, Holme PA, Mizobuchi M, Morales RJ, De Paula AM, Stray-Pedersen A, Lyle R, Dalhus B, et al. 2014. A Dominant STIM1 Mutation Causes Stormorken Syndrome. Hum Mutat.

Morin G, Bruechle NO, Singh AR, Knopp C, Jedraszak G, Elbracht M, Bremond-Gignac D, Hartmann K, Sevestre H, Deutz P, et al. 2014. Gain-of-Function Mutation in STIM1 (P.R304W) Is Associated with Stormorken Syndrome. Hum Mutat 35:1221-1232.

Muik M, Frischauf I, Derler I, Fahrner M, Bergsmann J, Eder P, Schindl R, Hesch C, Polzinger B, Fritsch R, et al. 2008. Dynamic coupling of the putative coiled-coil domain of ORAI1 with STIM1 mediates ORAI1 channel activation. J Biol Chem 283:8014-8022.

Navarro-Borelly L, Somasundaram A, Yamashita M, Ren D, Miller RJ, Prakriya M. 2008. STIM1-Orai1 interactions and Orai1 conformational changes revealed by live-cell FRET microscopy. J Physiol 586:5383-5401.

Nesin V, Wiley G, Kousi M, Ong EC, Lehmann T, Nicholl DJ, Suri M, Shahrizaila N, Katsanis N, Gaffney PM, et al. 2014. Activating mutations in STIM1 and ORAI1 cause overlapping syndromes of tubular myopathy and congenital miosis. Proc Natl Acad Sci U S A.

Park CY, Hoover PJ, Mullins FM, Bachhawat P, Covington ED, Raunser S, Walz T, Garcia KC, Dolmetsch RE, Lewis RS. 2009. STIM1 clusters and activates CRAC channels via direct binding of a cytosolic domain to Orai1. Cell 136:876-890.

Parvez S, Beck A, Peinelt C, Soboloff J, Lis A, Monteilh-Zoller M, Gill DL, Fleig A, Penner R. 2008. STIM2 protein mediates distinct store-dependent and store-independent modes of CRAC channel activation. FASEB J 22:752-761.

Picard C, McCarl CA, Papolos A, Khalil S, Luthy K, Hivroz C, LeDeist F, Rieux-Laucat F, Rechavi G, Rao A, et al. 2009. STIM1 mutation associated with a syndrome of immunodeficiency and autoimmunity. N Engl J Med 360:1971-1980.

Salviati G, Pierobon-Bormioli S, Betto R, Damiani E, Angelini C, Ringel SP, Salvatori S, Margreth A. 1985. Tubular aggregates: sarcoplasmic reticulum origin, calcium storage ability, and functional implications. Muscle Nerve 8:299-306.

Stathopulos PB, Li GY, Plevin MJ, Ames JB, Ikura M. 2006. Stored Ca2+ depletion-induced oligomerization of stromal interaction molecule 1 (STIM1) via the EF-SAM region: An initiation mechanism for capacitive Ca2+ entry. J Biol Chem 281:35855-35862.

Thompson JL, Shuttleworth TJ. 2013. How many Orai's does it take to make a CRAC channel? Sci Rep 3:1961.

Vig M, Beck A, Billingsley JM, Lis A, Parvez S, Peinelt C, Koomoa DL, Soboloff J, Gill DL, Fleig A, et al. 2006. CRACM1 multimers form the ion-selective pore of the CRAC channel. Curr Biol 16:2073-2079.

Walter MC, Rossius M, Zitzelsberger M, Vorgerd M, Muller-Felber W, Ertl-Wagner B, Zhang Y, Brinkmeier H, Senderek J, Schoser B. 2015. 50 years to diagnosis: Autosomal dominant tubular aggregate myopathy caused by a novel STIM1 mutation. Neuromuscul Disord 25:577-584.

Zhang SL, Yeromin AV, Hu J, Amcheslavsky A, Zheng H, Cahalan MD. 2011. Mutations in Orai1 transmembrane segment 1 cause STIM1-independent activation of Orai1 channels at glycine 98 and channel closure at arginine 91. Proc Natl Acad Sci U S A 108:17838-17843.

Zheng H, Zhou MH, Hu C, Kuo E, Peng X, Hu J, Kuo L, Zhang SL. 2013. Differential roles of the C and N termini of Orai1 protein in interacting with stromal interaction molecule 1 (STIM1) for Ca2+ release-activated Ca2+ (CRAC) channel activation. J Biol Chem 288:11263-11272.

Zhou Y, Ramachandran S, Oh-Hora M, Rao A, Hogan PG. 2010. Pore architecture of the

ORAI1 store-operated calcium channel. Proc Natl Acad Sci U S A 107:4896-4901.

Accepted Article

30

FIGURE LEGENDS

Figure 1 - Histological, ultrastructural, and immunohistochemical characterization of the biopsies

(A) Muscle biopsies from patients from all three families display tubular aggregates appearing in red on Gomori trichrome and in dark blue on NADH-TR staining in both fiber types. The aggregates are barely detectable with SDH. Minor fiber size variability and internalized nuclei are also noted. Ultrastructural analyses demonstrate that the tubular aggregates are of variable size and consist of single or double-walled membranes of different diameter. EM pictures were not available for Family 2. (B) Immunolocalization studies on biopsies from Family 1 and Family 2 show that the tubular aggregates contain STIM1, RYR1, SERCA, whereas ORAI1 is barely or not trapped. Note that STIM1 signals are found in the periphery and in the center of the aggregates, while RYR1 is mainly found in the periphery (arrows). * indicate identical fibers of serial sections.
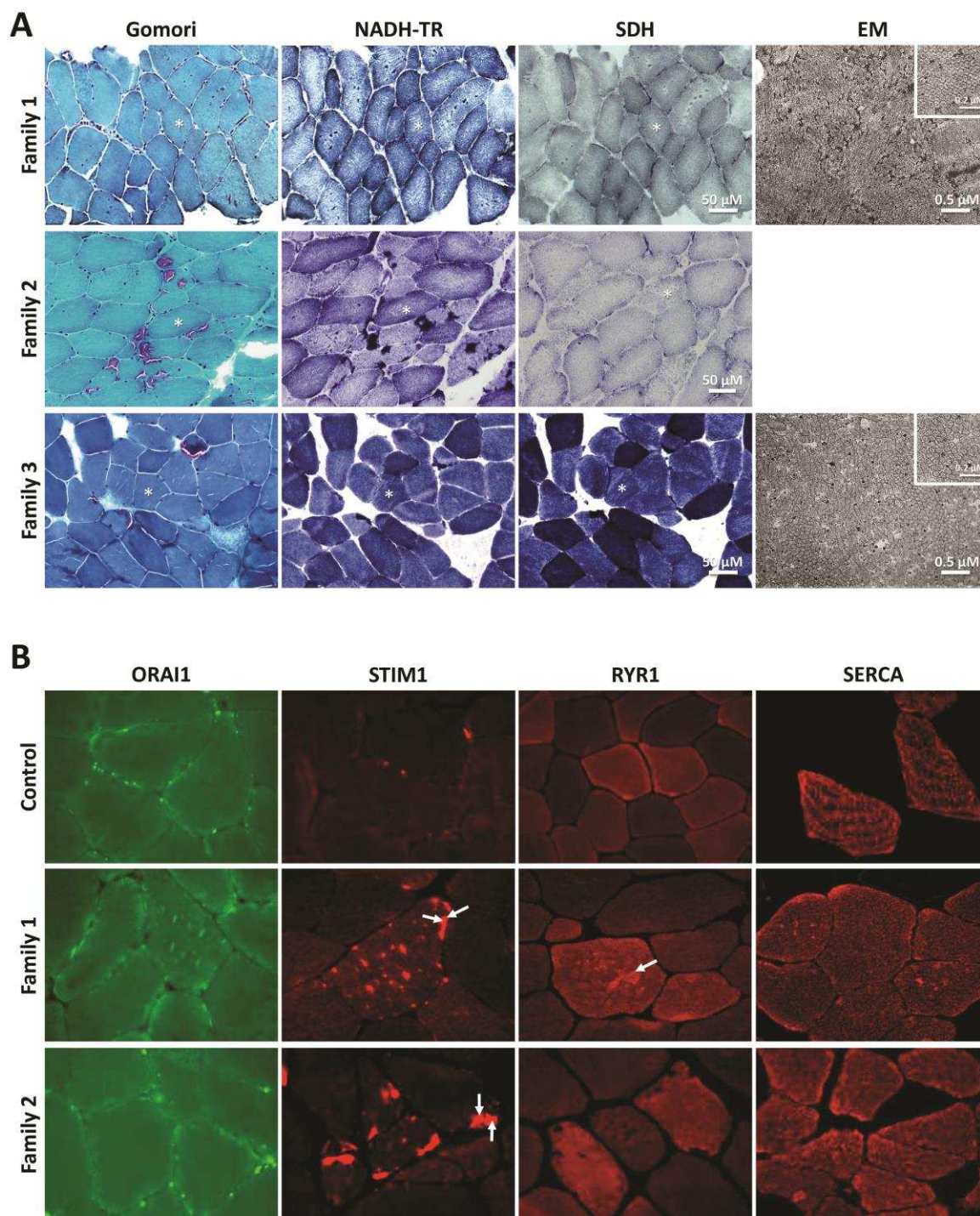
Figure 1

Figure 2 - Identification of *ORAI1* mutations

(A) Heterozygous *ORAI1* missense mutations were identified in all three families, and segregated with the disease. (B) The mutations affect highly conserved amino acids in ORAI1. (C) Schematic representation of ORAI1. Mutations found in our patients are depicted in blue, published mutations appear in red. G98S and V107M affect amino acids in transmembrane domain 1 (M1), and T84M affects an amino acid in M3. Residue G98 is located in the rigid section of the channel, and V107 neighbors the Ca^{2+} selectivity filter E106.
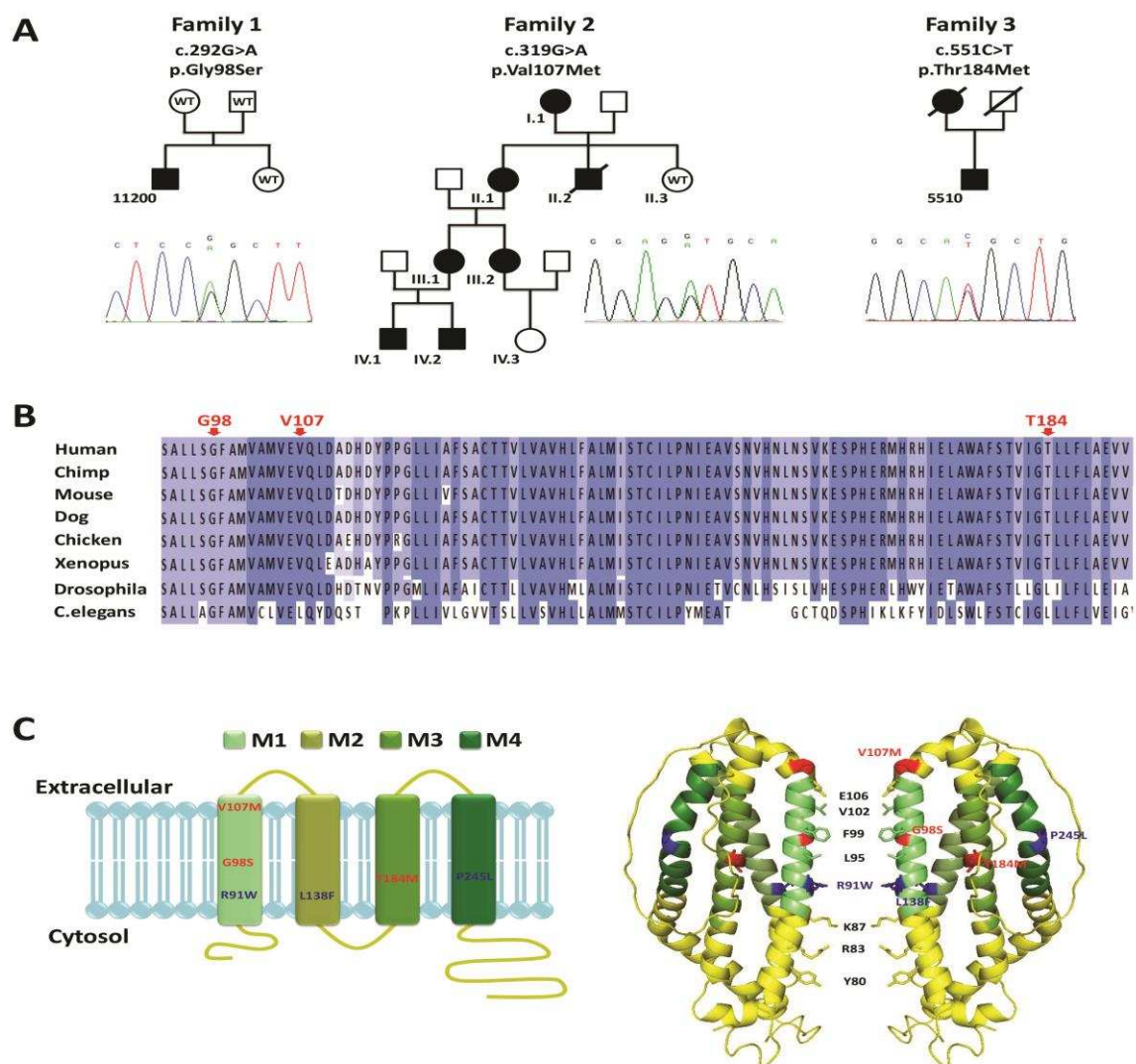

Figure 2

Figure 3 - Effect of *ORAI1* mutations on channel localization and clustering at the PM

(A) TIRF images of HEK-293T co-expressing STIM1 and wild-type (WT) or mutated (V107M, T184M, G98S) ORAI1-eGFP taken before and 10 min after addition of 1 µM Thapsigargin (Tg). Insets show cluster morphology at higher magnification. (B) Changes in intensity of eGFP clusters and in cluster density (% PM covered by clusters) in the TIRF plane following Tg addition in cells co-expressing STIM1 and WT or mutated ORAI1-eGFP. (C) Statistical evaluation of eGFP cluster intensity and density before and after Tg treatment. Data are mean ± SEM of 33, 24, 25, and 14 cells for WT, V107M, T184M and G98S, respectively. No statistically significant differences were observed between WT and mutated channels in resting and store-depleted conditions.
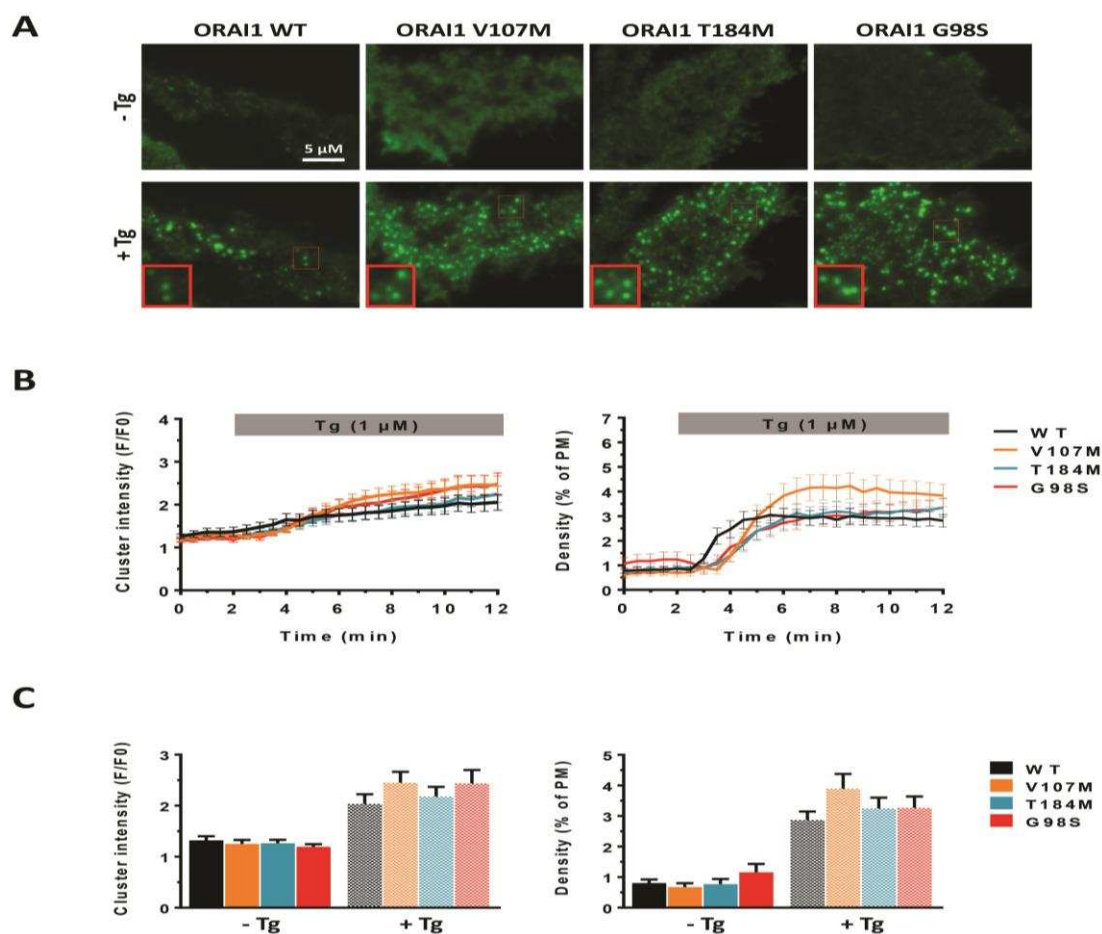
34

Figure 4 - Effect of *ORAI1* mutations on basal Ca^{2+} level

(A) Representative Fura-2 recordings of HEK-293T cells expressing wild-type (WT) or mutated (V107M, T184M) ORAI1-eGFP during Ca^{2+} removal (2 mM Ca^{2+} replaced by 1 mM EGTA). (B) Recordings of cells expressing WT or G98S ORAI1-eGFP during Ca^{2+} removal and readmission. Cells were cultured in a Ca^{2+}-poor medium (0.2 mM) to mitigate the toxicity associated with the G98S mutation. (C) Statistical evaluation of the responses illustrated in (A) and (B), measured between the time points indicated with # (n = 79, 39, 49 for WT, V107M, T184M respectively, and n = 38, 20 for WT and G98S cultured in low Ca^{2+}). (D), (E) Representative Mn^{2+} quench recordings of MEF-DKO cells (*Stim1$^{-/-}$/Stim2$^{-/-}$*) expressing WT or mutated ORAI1-eGFP. Fura-2 fluorescence was recorded at 360 nm in the presence of 2 mM Ca^{2+}. Traces are offset to facilitate comparison. (F) Statistical evaluation of Mn^{2+} quench rates in (D) and (E), measured between the time points indicated with # (n = 17, 20, 21 and 23, 32 for WT, V107M, T184M, and WT, G98S cultured in low Ca^{2+}, respectively). Data are mean ± SEM, statistically significant differences versus respective WT conditions are indicated by **** p < 0.0001.
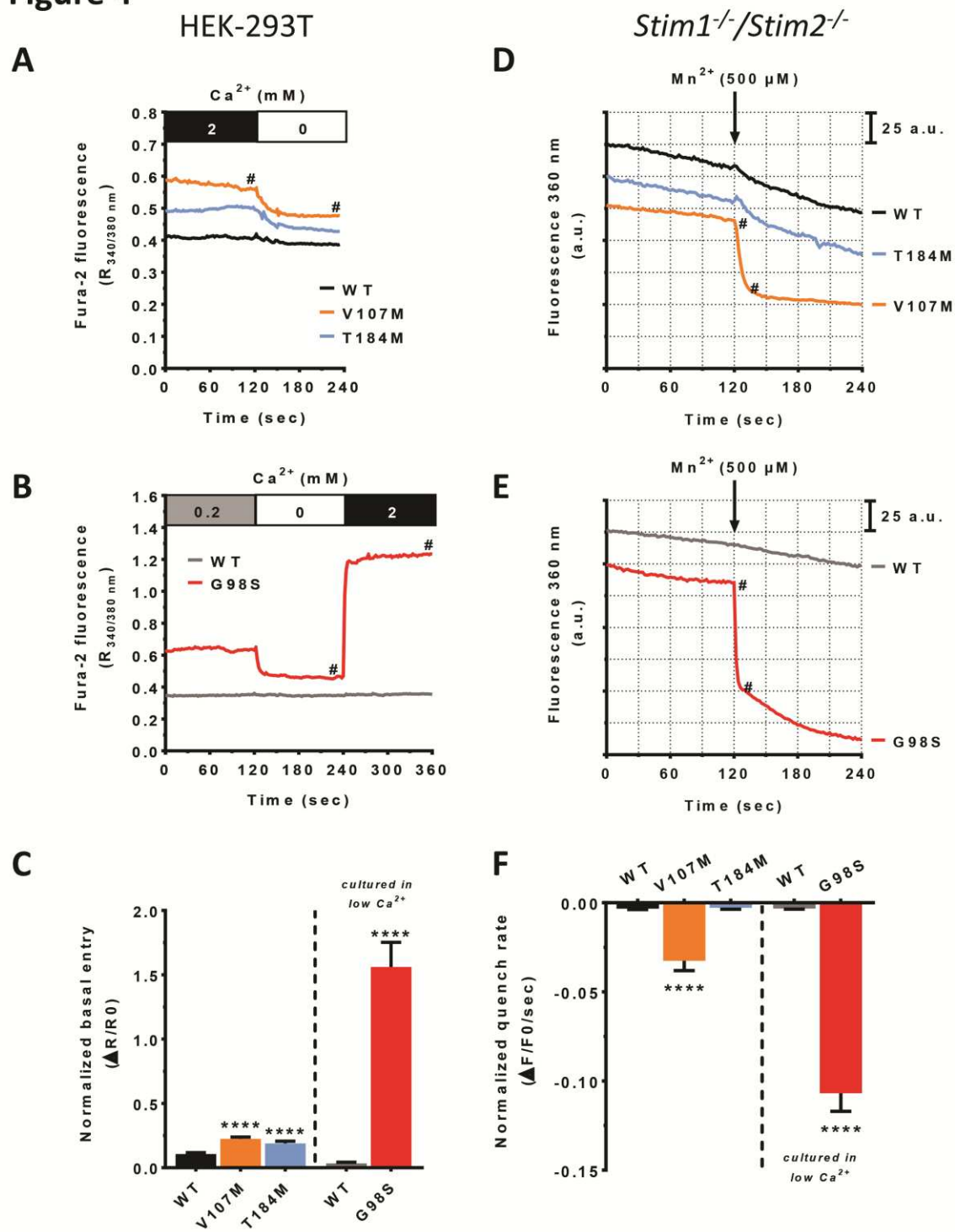
Figure 4

HEK-293T

A

B

C

Stim1$^{-/-}$/Stim2$^{-/-}$

D

E

F

Figure 5 - Effect of *ORAI1* mutations on maximal SOCE

(A), (D) Fura-2 responses evoked by the readmission of 0.5 mM Ca^{2+} (HEK-293T) or 2 mM Ca^{2+} (MEF-DKO) to cells co-expressing mCherry-STIM1 and ORAI1-eGFP (WT, V107M, T184M or G98S) treated with Tg. (B), (E) Statistical evaluation of the influx rate evoked by Ca^{2+} readmission in (A) and (D), measured as the Fura-2 increase slope between the time points indicated with #. (C), (F) Statistical evaluation of the Ca^{2+} level 60 seconds after the peak of the response in (A) and (D), illustrated by the dotted line, and expressed as percentage of the peak. Data are mean ± SEM of 24-51 cells for (B), (C) and of 17-29 cells for (E), (F). Statistically significant differences versus respective WT conditions are indicated by ** $p < 0.01$, *** $p < 0.001$, and **** $p < 0.0001$.
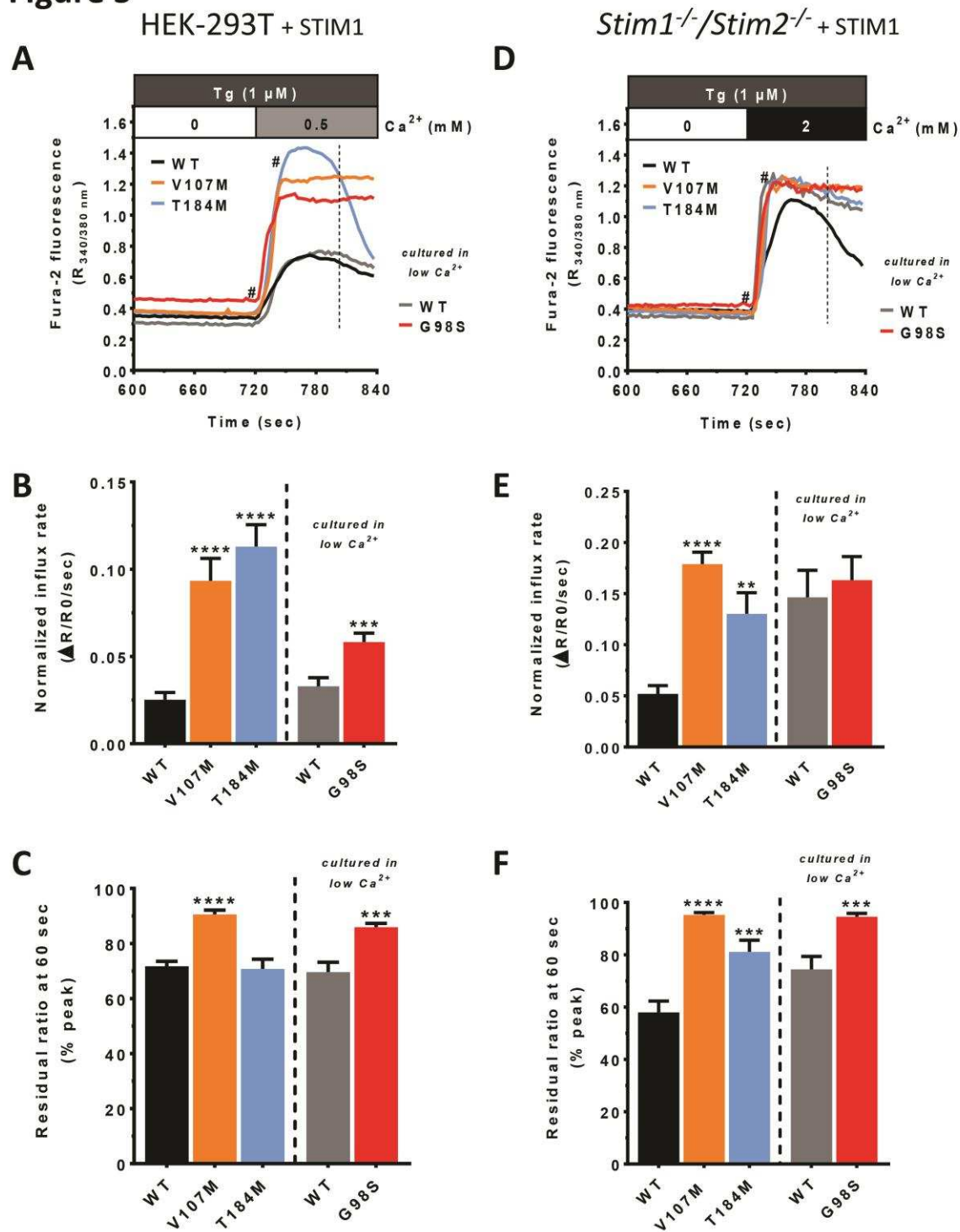
Figure 5

Table 1. Genetic, clinical and histological features in patients with *ORAI1* mutations

	Family 1	Family 2							Family 3
Individual	11200	I.1	II.1	II.2	III.1	III.2	IV.1	IV.2	5510
Gender	M	F	F	M	F	F	M	M	M
Mutation	c.292G>A p.Gly98Ser	c.319G>A p.Val107Met	c.319G>A p.Val107Met	c.319G>A p.Val107Met	c.319G>A p.Val107Met	c.319G>A p.Val107Met	c.319G>A p.Val107Met	c.319G>A p.Val107Met	c.551C>T p.Thr184Met
Onset	childhood	unknown	childhood	unknown	childhood	childhood	childhood	childhood	adulthood
Age at last examination	10	no examination	47	no examination	25	31	8	6	60
Muscle symptoms	proximal and distal weakness of lower limbs, myalgia, cramps, stiffness	NA	stiffness, cramps	NA	proximal weakness of lower limbs, exercise-induced myalgia	weakness of arms, cramps	myalgia, stiffness	myalgia	mild general weakness, myalgia in lower limbs, cramps
Walking	tip-toe walking, waddling gait	NA	tip-toe walking, difficulty climbing stairs	NA	tip-toe walking, difficulty climbing stairs	tip-toe walking	tip-toe walking	normal	normal
Contractures	elbows, Achilles tendons	NA	Achilles tendons	NA	Achilles tendons	NA	Achilles tendons	Achilles tendons	no
CK level (U/I)	2052	NA	791	NA	1383	597	1538	484	600

normal range 60-180									
Histology	TAs in type I/II fibers, fiber size variability, internalized nuclei	NA	TAs in type I/II fibers, fiber size variability, internalized nuclei	NA	NA	NA	NA	NA	TAs in type I/II fibers, fiber size variability, internalized nuclei
Signs of Stormorken syndrome	ichtyosis, miosis, bleeding episodes	NA	no	NA	no	no	dyslexia	dyslexia	no
Other features	occasional mild hypocalcemia	COPD, cerebrovascular disease	no	NA	calf hypertrophy	no	calf hypertrophy, seizures	calf hypertrophy, scapular winging	hypereosinophilia, pectus excavatum, arched palate

NA = not assessed